Journal of Thermal Analysis and Calorimetry (2019) 138:4295–4302
https://doi.org/10.1007/s10973-019-08715-6

Influence of barium oxide on glass-forming ability and glass stability of the tellurite–phosphate oxide glasses

Thermal and structural investigations

M. Leśniak[1] · R. Szal[1] · B. Starzyk[1] · M. Gajek[1] · M. Kochanowicz[2] · J. Żmojda[2] · P. Miluski[2] · J. Dorosz[2] · M. Sitarz[1] · D. Dorosz[1]

Received: 18 October 2018 / Accepted: 16 August 2019 / Published online: 28 August 2019

Abstract
The effect of BaO content on the glass-forming ability, glass stability and structure of tellurite–phosphate oxide glasses in the $70TeO_2$–$10P_2O_5$–(20-x)ZnO–xBaO (x = 0, 5 and 10 mol%) system has been discussed. From the differential scanning calorimetry, the glass transition (Tg), crystallization (Tc) and the melting (Tm) temperatures were estimated. The decrease in reduced glass transition temperature (Tr_g) and glass-forming tendency parameter ($K_h(Tc_1)$) with addition and increasing BaO caused a decrease in the glass-forming ability of glasses. It was also found that the thermal stability of these glasses against crystallization decreased with increase in BaO concentration into chemical composition of base glass, i.e., glass without barium oxide. The FTIR spectra were measured to understand the structure of the obtained tellurite–phosphate oxide glasses. The results have shown that phosphorous and tellurium ions were taken part in the formation of the glass network of the studied glasses. The addition of BaO caused significant changes in the FTIR spectra of glasses. More and more TeO_3 and $TeO_{3+\delta}$ units and PO_4^{2-} groups (Q^1 units) were created when the BaO was added into the chemical composition of the base glass. Increasing barium ions content into the chemical composition of glasses caused depolymerization of the tellurite–phosphate oxide glass network.

Keywords Tellurite–phosphate oxide glasses · BaO · Glass-forming stability · Glass stability · Structure

Introduction

Recently, tellurite glasses have received considerable attention for their potential application as promising materials used for optical devices [1–5]. Tellurite glasses are characterized by good chemical durability, high luminescence intensity, low glass transition, good chemical resistance and high linear and nonlinear refractive index [3–5]. The low phonon energy (750 cm^{-1}) of tellurite glass is also attractive for designing near-IR and mid-IR lasers, amplifiers, and passive fibers for power delivery and sensor engineering [6–12]. It has been reported that up-conversion enhancement in zinc tellurite glass doped with Er^{3+} ions [13]. Walas et al. reported that tellurite glasses having erbium and dysprosium are good materials for a white light emission [14].

The tellurite glass structure is based on its parent crystalline forms: the α and β allotropic forms [5, 15, 16]. A number of investigations on the glass formation and structural analysis of binary and tellurite glasses have been reported [5, 17–21]. There are two basic structural units: TeO_4 (trigonal bipyramid), TeO_3 (trigonal pyramid), as well as the intermediate $TeO_{3+\delta}$ polyhedron [5, 16, 22]. In TeO_4 unit, four oxygen atoms are coordinated with one tellurium atom to form a trigonal bipyramid (tbp) with one of the equatorial oxygen positions unoccupied [5, 16, 23, 24]. In the trigonal pyramid structure, there are

✉ M. Leśniak
mlesniak@agh.edu.pl

[1] AGH University of Science and Technology, av. Mickiewicza 30, Kraków, Poland

[2] Bialystok University of Science and Technology, 45A, Wiejska Street, Białystok, Poland

two bridging oxygen sites and one non-bridging oxygen (NBO) which is a Te = O double bond [5, 16, 25]. This is a unique structural characteristic of TeO_2 glass, distinct from other network-forming glasses; e.g., silicates, phosphates and germanates in which only the NBO and bridging oxygen exist as a part of the structural unit [5, 16, 26–29]. Modifiers such as BaO and ZnO break the random network of glasses, and the concentration of TeO_3 and $TeO_{3+\delta}$ units increases [30].

An extensive list of tellurite glass compositions with glass-forming ranges is reported in literature [17–20]. There are a large number of strongly covalent glass-forming oxides (B_2O_3, P_2O_5, GeO_2), and intermediates formers (WO_3, Nb_2O_5, V_2O_5) combine with TeO_2 [17–20, 24, 31, 32]. Although attractive properties of tellurite glasses have been revealed, few studies have been made on the compositional dependence of basic properties such as glass-forming and thermal properties, which are essential for the design of glass materials. The tellurium–germanate glasses are also a potential glass host for optical fibers [33, 34]. Germanium-based glasses possess higher phonon energy in comparison with tellurium-based glasses. However, germanium-based glasses are characterized by higher thermal stability and higher mechanical strength than tellurium-based glasses [35]. The barium gallo-germanate glasses modified with tellurium oxide were studied as a potential glass host for Eu^{3+} ions to induce emission in the UV region. Significant addition of tellurium oxide to the glass set causes host glass structure polymerization and a decrease in emission intensity [36]. Last authors' results suggested that modification of tellurite glasses with germanium oxide may be a perspective approach into efficient luminescent optical fiber light sources. However, key parameters are the control of viscosity and crystal nucleation and growth which tends to minimize the extrinsic scattering loss due to the presence of crystals during glass preform and fiber fabrication [19]. Further examinations in the glass–ceramic in the system of TeO_2-GeO_2 will be performed in order to obtain a laser emission and second harmonic generation [37, 38]. Glass features mentioned above can be controlled by the analysis of the thermal properties and for that purposes, differential scanning calorimetry (DSC) is commonly used [19, 29]. Liu et al. [39] reported the glass transition and devitrification characteristics of two different families of glass-forming systems: NZT [$(90\text{-}x)TeO_2$–$10ZnO$–xNa_2O, x = 50, 10, 20 and 30 mol%)] and TZX [$70TeO_2$–$10ZnO$–$20X$, X = 5ZnO, Li_2O, Na_2O and K_2O]. In general, the absence of alkali oxides tends to lower the thermal stability of tellurite glass. By incorporating alkali oxide in the tellurite glass compositions, the glass stability increases as determined. It is evident that the presence of Na_2O in the TZN glass system is essential for reducing the crystallization tendency when the TeO_2/Na_2O ratio is lower than 2:1 [39]. For a sodium–tellurite composition, the highest value of Hrubby parameter was found for 20 mol% of Na_2O, which is why this composition was modified by incorporating 10 mol% ZnO [40]. According with Kaur et al. [30], as the concentration of BaO increases in xBaO–$(100\text{-}x)TeO_2$ (where x = 10, 15 and 20 mol%) from 10 to 20 mol%, the value of ΔT decreases from 140 °C to 100 °C. Therefore, the thermal stability of glasses against crystallization decreases.

Phosphate gasses have shown better thermal stability and tensile strength than tellurite glasses. For these reasons, tellurite–phosphate glasses have received increasing attention with the goal to find a good compromise between the pure tellurite and phosphate glass properties [41]. Konishi et al. [42] were first to report a phase diagram in the ternary TeO_2–P_2O_5–ZnO system. The authors investigated the glass-forming region, the compositional dependence of the glass transition temperature and the coloring property for these (PTZ) systems. Konishi et al. [42] concluded that ZnO in all glass samples acts as a network former which bridges between the PO_4 and TeO_4 chains so that the glass transition temperature increases with the increase in ZnO content.

Apart from applications of tellurite–phosphate glasses, there is a lack of data on structural investigations as well as the thermal properties of these glass systems in the literature. Therefore, the aim of this research is to study the effect of barium on the thermal properties and structure of tellurite–phosphate glass system in order to understand the fundamental origin of such properties.

In the present work, the main aim was to study the glass-forming ability and glass stability parameters of the tellurite–phosphate glasses in the $70TeO_2$–$10P_2O_5$–$(20\text{-}x)$ZnO–xBaO (x = 0, 5 and 10 mol%) system. These parameters are formulated by different combinations of the following characteristic differential scanning calorimetry (DSC) temperatures: the glass transition temperature (Tg), the crystallization temperature (Tc) and the melting temperature (Tm). Additionally, FTIR spectra of glasses were analyzed in order to identify the contribution of each component to the local structure that determined the physical properties of these glasses.

Experimental

The glass samples with molar compositions of $70TeO_2$–$10P_2O_5$–$(20\text{-}x)$ZnO–xBaO (x = 0, 5 and 10 mol%) were successfully synthesized by the melt-quenching method. Samples were prepared by using tellurium dioxide (purity ≥ 99.0%), phosphate pentoxide (purity ≥ 99.9%), zinc oxide, ZnO (purity > 99.9%) and barium oxide (purity

99.9%). The powder chemicals were weighed using an electronic digital weighting machine with an error of ± 0.0001 g. Each batch was heated from room temperature to 850 °C at a rate 10° min^{-1} in PtIr crucible in the melting furnace in air atmosphere. The melt was held at maximum temperature for 20 min until a bubble-free liquid was formed. The homogeneous melt was quenched by pouring it onto a preheated stainless steel mold to avoid excess thermal shocks. The glasses were annealed for 2 h at 20 °C below than the glass transition temperature to release the mechanical strains. The transformation temperature was based on literature data [3, 30, 41].

The nature of each sample was confirmed by using X-ray diffraction (XRD). X-ray diffraction studies were carried out on powdered samples on X'Pert Pro X-ray diffractometer supplied by PANalytical with Cu $K\alpha_1$ radiation (λ = 1.54,056 Å) in the 2θ range of 10°–90°. The step size, time per step and scan speed were as follows: 0.017°, 184.79 s and 0.011° s^{-1}. The X-ray tube was operated at 40 kV and 40 mA, and a scintillation detector was used to measure the intensity of the scattered X-rays.

Microstructure observations of glasses were made using a scanning electron microscope SEM–FEI Nova 200 NanoSEM with an analyzer of the element composition in micro-areas (EDS).

The thermal characteristic temperatures such as the glass transition (Tg), the crystallization (Tc) and the melting (Tm) temperatures were measured by using a Jupiter DTA STA 449 F3 thermal analyzer supplied by NETZSCH thermal analysis, operating in heat flux DSC with a heating rate of 10 °C min^{-1} in the 260–760 °C temperature range. Characteristic temperatures have been determined at the peak maximum.

The FTIR absorption spectra of the glasses in the 520–1200 cm^{-1} range were obtained with a Fourier spectrometer (Bruker Optics-Vertex 70 V). The measurements were done using the KBr pellet technique. Absorption spectra were recorded at 128 scans and the resolution of 4 cm^{-1}.

The glass samples were labeled with the first letters of the components (TeO_2–T, P_2O_5–P, ZnO–Z, BaO–B) and in accordance with the BaO content, i.e., 0 mol% of BaO (TPZ0B), 5 mol% of BaO (TPZ5B) and 10 mol% of BaO (TPZ10B).

Results and discussion

Chemical composition of samples

After melting the glass samples, each sample was determined by visual inspection. All obtained samples were transparent and bubble free.

Table 1 The molar composition of samples

Glass sample	Molar composition/mol%			
	TeO_2	P_2O_5	ZnO	BaO
TPZ0B	70	10	20	0
TPZ5B			15	5
TPZ10B			10	10

Table 1 shows molar composition of all obtained samples. The started glass composition (TPZ0B), which was then modified by BaO (5 and 10 mol%), was selected from the glass-forming region presented in publication [42].

XRD analysis

The X-ray diffraction patterns of the all samples depicted in Fig. 1 were found to show no sharp peaks (characteristic for long-range atomic arrangement and the periodicity of the three-dimensional network) but broad halo at around 20°–35°, which reflected the characteristic of the amorphous glass structure.

SEM–EDS

SEM micrographs of solid glass pieces in Figs. 2–4 showed their homogeneous character, no liquidation and the non-presence of crystalline phases were observed. The white spots visible on SEM micrographs are artifacts.

As can be seen in the EDS spectra (Figs. 2–4), the glass matrix of all sample is a tellurite–phosphate phase with ions of alkaline earth metals.

Glass-forming ability parameters

The results of the DSC thermal analysis of the tested glasses are presented in Fig. 5, and Table 2. The transformation temperature Tg of all the tested glasses is about 377 °C and showed no significant differences after the introduction of BaO into the composition of the base glass. The DSC thermal measurements showed a high tendency for all glasses to crystallize. On the thermal curve of TPZ0B glass, one clear exothermic effect (491 °C) was observed, while on thermal curves of glasses with BaO addition, two exothermic effects were observed (Fig. 5). On the DSC curve of TPZ5B glass, the exothermic peak is visible at the maximum in 483 °C. The second weaker effect was recorded for the temperature 522 °C. As in the case of TPZ5B glass, the DSC curve of TPZ10B glass also shows two exothermic effects at the maximum, in 470 °C and 544 °C, respectively. In the obtained DSC curves, a shift of the maximum crystallization peak to higher

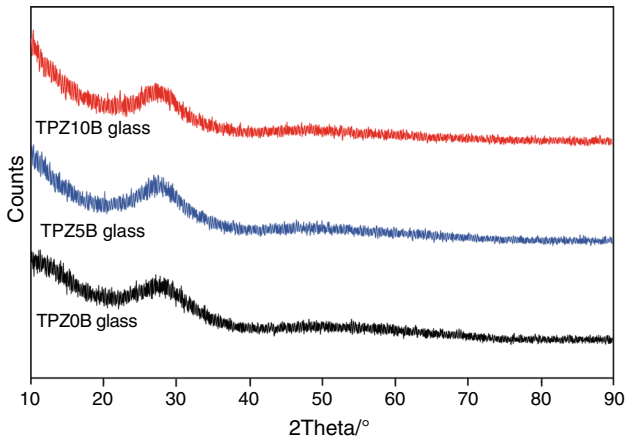

Fig. 1 The X-ray patterns of tellurite–phosphate glasses

temperatures was observed with the increase of BaO content. The endothermic melting effect for TPZ0B and TPZ5B glasses occurred at a temperature of 600 °C. In glass TPZ10B glass, a shift of the melting peak to 682 °C was observed (Fig. 5).

Several parameters or criteria have been proposed to reflect the relative glass-forming ability (GFA) among bulk glasses on the basis of different calculation methods [43, 44]. One is the reduced glass transition temperature T_{rg} = Tg/Tf_1 which is the ratio between the glass transition temperature Tg and the first melting temperature Tf_1 of the corresponding glass-forming system [45, 46]. Another parameter is also used as a measure of the glass-forming tendency of materials: $K_h = (Tc_1 - Tg)/(Tf_1 - Tc_1)$, where Tc_1 is the first crystallization temperature [47].

Using the data shown in Fig. 5 and Table 2, the reduced glass transition temperature (Tr_g) values for glasses vary from 0.62 (TPZ0B) to 0.55 (TPZ10P). For glasses containing a concentration of barium oxide, $K_h(Tc_1)$ parameter decreases from 0.20 to 2.33 as shown in Table 2. The decrease in Tr_g and $K_h(Tc_1)$ parameters with addition and with increase in BaO no incorporation supports the glass-

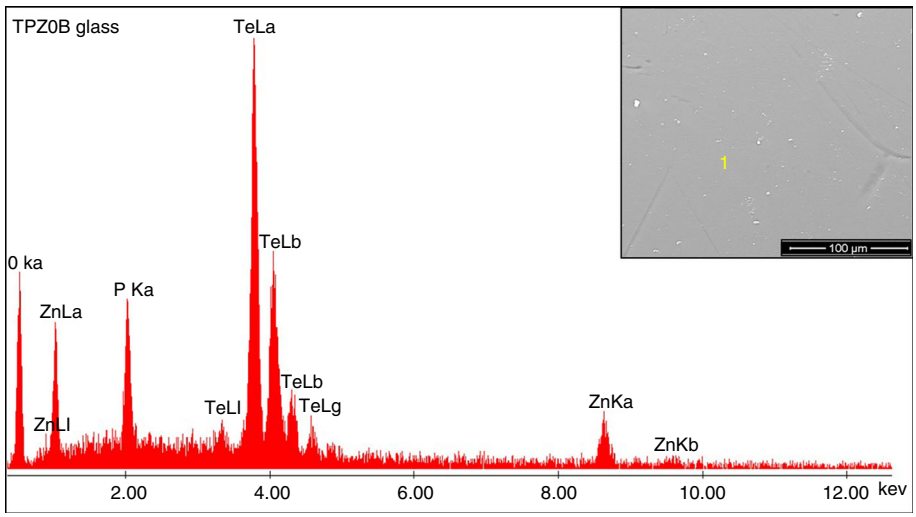

Fig. 2 SEM micrograph of TPZ0B glass with EDS analysis in point 1

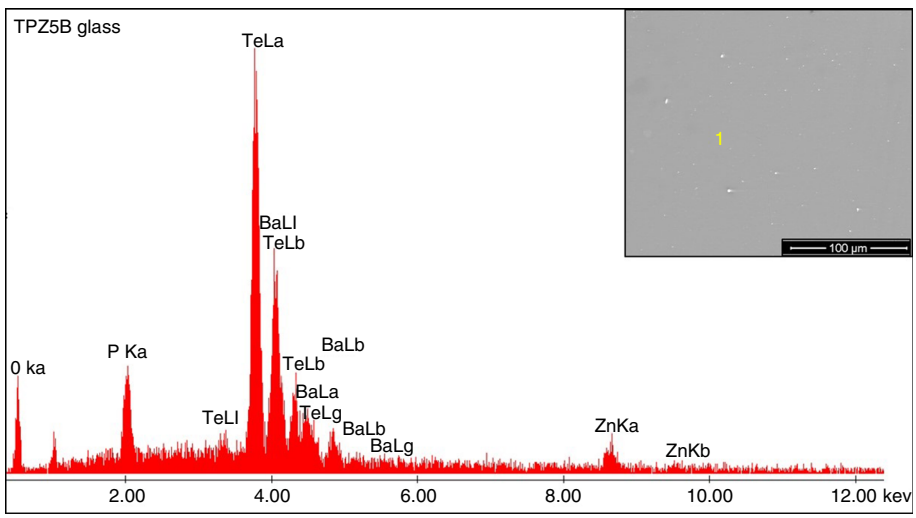

Fig. 3 SEM micrograph of TPZ5B glass with EDS analysis in point 1

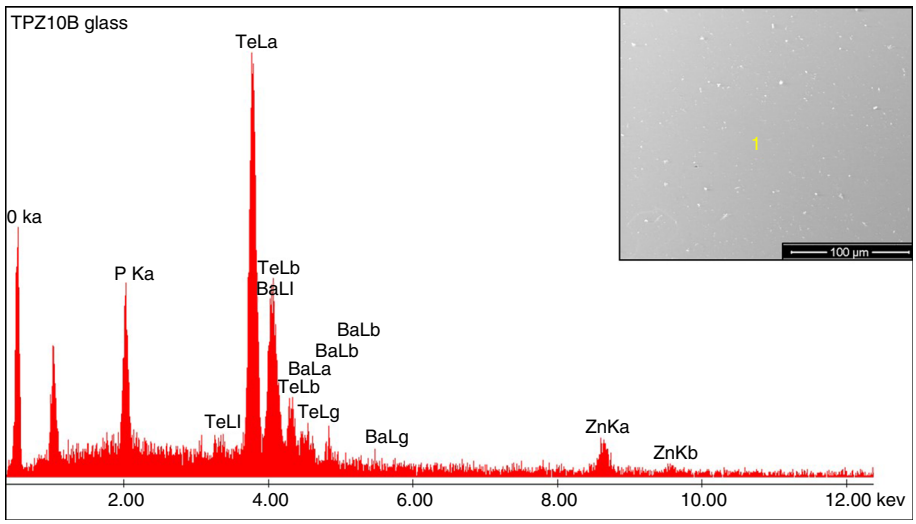

Fig. 4 SEM micrograph of TPZ10B glass with EDS analysis in point 1

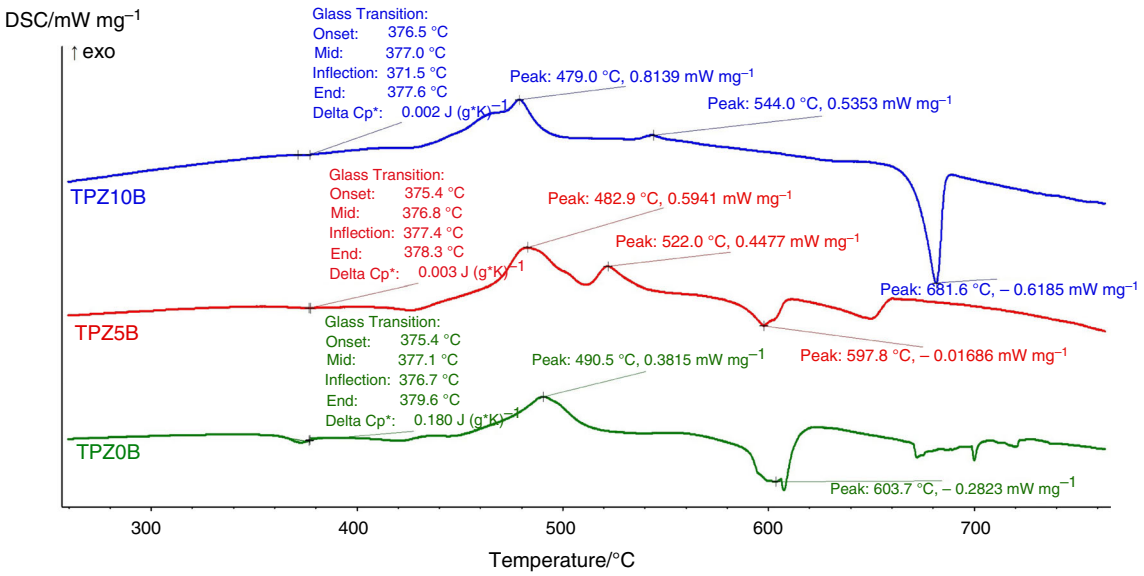

Fig. 5 The DSC curves of tellurite–phosphate glasses

Table 2 The thermal properties (Tg, Tc_1 and Tm_1) from DSC curves, values of glass-forming ability parameters (Tr_g and K_h) and values of glass-forming stability parameters (K_w, K_1 and ΔT)

Sample	Tg (°C)	Tc_1	Tc_2	Tm_1	Tr_g	$K_h(Tc_1)$	$K_w(Tc_1)$	$K_1(Tc_1)$	$\Delta T(Tc_1)$ (°C)
TPZ0B	377	491	–	604	0.62	1.01	0.19	0.51	114
TPZ5B	377	483	522	598	0.63	0.92	0.18	0.50	106
TPZ10B	377	479	544	682	0.55	0.50	0.15	0.45	102

forming ability. The GFA decreases with a decrease in BaO concentration.

Glass stability parameters

For the studied glasses, the glass stability parameters were also estimated by $K_w = (Tc_1 - Tg)/Tf_1$ [48, 49], $K_1 = Tc_1/(Tg + Tf_1)$ [43, 44] and $\Delta T = Tc_1 - Tg$ [45].

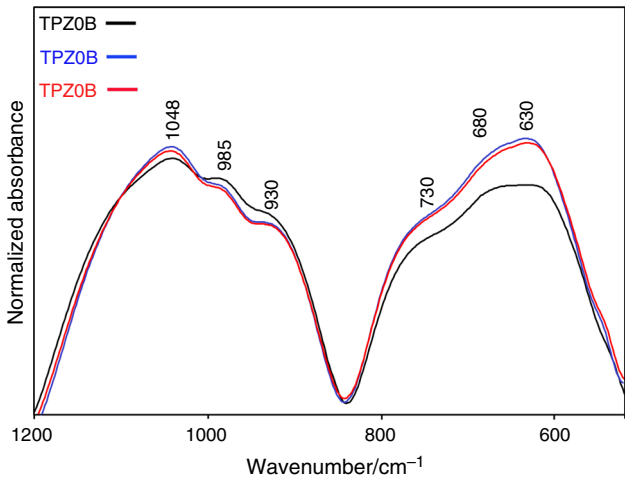

Fig. 6 FTIR spectra of tellurite–phosphate glasses

Values of $K_w(Tc_1)$ parameter and parameter $K_l(Tc_1)$ decrease when BaO concentration is added in the ternary system TeO_2–P_2O_5–ZnO (Table 2). Generally, the difference, $\Delta T(Tc_1) = Tc_1 - Tg$, gives a measure of the thermal stability of the glass [45]. For the present study, its values are found to be 114 °C on the ternary system TeO_2–P_2O_5–ZnO and 106–102 °C on the four-component system (containing 5 and 10 mol% BaO). It is obvious that the thermal stability of these glasses against crystallization decreased with increase in BaO concentration.

FTIR spectroscopy study

The FTIR spectra of the tellurite–phosphate oxide glasses were measured in the 1200–520 cm^{-1} range and are shown in Fig. 6. The FTIR spectra of all prepared samples showed bands typical of tellurite glasses, i.e., at around 630 cm^{-1}, 680 cm^{-1} and 730 cm^{-1} [14, 15, 50]. The all spectra showed also major bands in 900–1200 cm^{-1} range, characteristic of the phosphate network [51]. It confirms that the network of glasses contains two network formers, i.e., tellurium and phosphate oxides.

The assignment of the FTIR bands was performed based on the literature available on the tellurite, phosphate and tellurite–phosphate oxide glasses [14, 15, 50–52].

The bands at around 630 cm^{-1} and 680 cm^{-1} are due to the Te–O stretching vibration in TeO_3 and $TeO_{3+\delta}$ units, respectively, whereas band at 730 cm^{-1} is due to stretching vibrations of P–O–P vibrations in Q^1 units, (1: number of link) (Fig. 6) [14, 15, 52].

Taking into account the FTIR results reported about some phosphate glasses may be assumed that the bands centered at around 930 cm^{-1} and 985 cm^{-1} are due to the P-O-P asymmetric stretching vibrations in Q^2 units [50] and band at around 1048 cm^{-1} is assigned to the stretching vibrations of the PO_4^{2-} groups (Fig. 6) [50–52].

As is shown in Fig. 6, the addition of BaO caused significant changes in the FTIR spectra of glasses. The intensity of the band at around 630 cm^{-1} and 680 cm^{-1} increased with addition and increase in BaO content in the base glass, as expected, since there are lower Te–O–Te linkages. This means that more non-bridging units are formed in the tellurite–phosphate network [30, 53, 54]. The addition of barium oxide contributed to a decrease in the intensity of the bands at around 930 cm^{-1}, 985 cm^{-1} and an increase in the intensity of the band at 1048 cm^{-1}. In fact, more and more PO_4^{2-} groups (Q^1 units) were created, when the BaO was added to the chemical composition of TPZ glass.

Discussion

Characteristic temperatures, such as transition, crystallization and melting temperatures, play an important role in understanding the physical properties of glasses. Glasses with a close-packed network will have thermal stability, while those with loose-packed network will have instability [55]. Generally, the Ba^{2+} ions are incorporated into the glass network as modifier ions, resulting in the loose packing of the glass network. Sekiya et al. [56] have been suggested that the binary tellurite glasses containing less than 20 mol% of BaO have a continuous network composed of TeO_4 tbps, TeO_{3+1} polyhedra and TeO_3 tps sharing vertices. In these glasses, an increase in BaO content promoted conversion of TeO_4 tbps into TeO_{3+1} polyhedra and TeO_3 tps. These data have also been confirmed by Sokolow et al. [57] and Kaur et al. [30]. Modifier ions such as Ba^{2+} ions broke the random network of glasses, and the concentration of TeO_3 tps and TeO_{3+1} polyhedra increased [57]. The decrease in transition temperature value with increase in Ba^{2+} ions content contributes to a decrease in thermal stability of the glasses leading to loose-packed network [30]. The decrease in the glass transition temperature values implies that the number of bridging oxygen groups decreases. This is mainly due to the addition of BaO which weakens the bond between each atom glass, increasing the number of NBOs atoms. The bond is easier to break, and hence, the transition temperature of the glass decreased. It also implies a decrease in rigidity of the glass network [30, 55]. In our study, the addition of BaO in TeO_2-P_2O_5 network no caused the decreasing values of the transition temperature. Also, the glass-forming ability parameters and glass stability parameters decreased when Ba^{2+} ions were incorporated in the structure of TPZ glass. Probably, it is due to the change in the network of glasses, i.e., more non-bridging $Te–O^-$ units and PO_4^{2-} groups are formed in the tellurite–phosphate network when the BaO was added to the chemical

composition of base glass. The evolution of the network can be explained by the depolymerization of tellurite–phosphate glass network. The phosphate chain length decreased in the glasses with high BaO content due to the depolymerization of the tellurite–phosphate network, leading to an increase in the number of short phosphate chain units or rings [52]. The addition of barium oxide also increased the TeO_3 and $TeO_{3+\delta}$ units, at the expense of TeO_4 units. This consequently led to a decrease in the average cross-link density and the number of bonds per unit volume, which have a direct relation with characteristic temperatures of glasses. In this way, the thermal stability of these glasses against crystallization decreased with increase in BaO concentration and barium oxide no incorporation supports the glass-forming ability of glasses.

Conclusions

Tellurite–phosphate glasses without and with 5 and 10 mol% of BaO were prepared and characterized by differential scanning calorimetry (DSC) and FTIR spectroscopy. All presented glasses after heat treatment were fully amorphous materials. The crystalline phases were found as transition phases that dissolved above 590 °C in the tellurite–phosphate liquid during heat treatment.

Based on spectroscopic studies, it was found that barium ions are present in the network of the studied glasses as modifying ions that depolymerized the glass network. This led to a weakening of the tellurite–phosphate network and increase in the PO_4^{2-}, TeO_3 and $TeO_{3+\delta}$ units. It resulted in a reduction of glass-forming ability and glass stability of the tellurite–phosphate glasses when the BaO was added to the TeO_2–P_2O_5 system.

Acknowledgements The work is the result of the Research Project No. 2016/23/B/ST8/00706 funded by the National Science Centre, Poland.

References

1. Gonçalves A, Zanuto VS, Flizikowski GAS, Medina AN, Hegeto FL, Somer A. Luminescence and upconversion processes in Er^{3+}-doped tellurite glasses. J Lumin. 2018;201:110–4.
2. Venkataiah G, Babu P, Martín IR, Venkata Krishnaiah K, Suresh K, Lavín V. Spectroscopic studies on Yb^{3+}-doped tungsten-tellurite glasses for laser applications. J Non-Cryst Solids. 2018;479:9–15.
3. Dousti MR, Amjad RJ, Sahar MR, Zabidi ZM, Alias AN, de Camargo ASS. Er^{3+}-doped zinc tellurite glasses revisited: concentration dependent chemical durability, thermal stability and spectroscopic properties. J Non-Cryst Solids. 2015;429:70–8.
4. Kochanowicz M, Dorosz D, Zmojda J, Dorosz J, Miluski P. Influence of temperature on upconversion luminescence in tellurite glass co-doped with Yb^{3+}/Er^{3+} and Yb^{3+}/Tm^{3+}. J Lumin. 2014;151:155–60.
5. El-Mallawany RAH. Tellurite glass handbook: physical properties and data. Boca Raton: CRC Press; 2002.
6. Li D, Xu W, Kuan P, Li W, Lin Z, Wang X. Spectroscopic and laser properties of Ho^{3+} doped lanthanum-tungsten-tellurite glass and fiber. Ceram Int. 2016;42:10493–7.
7. Yang Z, Wu Y, Yang K, Xu P, Zhang W, Dai S. Fabrication and characterization of Tm^{3+}-Ho^{3+} co-doped tellurite glass microsphere lasers operating at ~ 2.1 μm. Opt Mater. 2017;72:524–8.
8. Su X. Energy transfer induced 2.0 μm luminescent enhancement in $Ho^{3+}/Yb^{3+}/Ce^{3+}$ tri-doped tellurite glass. J Lumin. 2018;203:26–34.
9. Sokolov VO, Plotnichenko VG, Koltashev VV, Dianow EM. On the structure of tungstate–tellurite glasses. J Non-Cryst Solids. 2006;352:5618–32.
10. El-Mallawany R. Tellurite glass smart materials: applications in optics and beyond. Cham: Springer; 2018.
11. Haouari M, Maaoui A, Saad N, Bulou A. Optical temperature sensing using green emissions of Er^{3+} doped fluoro-tellurite glass. Sens Actuators A Phys. 2017;261:235–42.
12. Manzani D, Flávio da Silveira Petruci J, Nigoghossian K, Cardoso AA, Ribeiro SJL. A portable luminescent thermometer based on green up-conversion emission of Er^{3+}/Yb^{3+} co-doped tellurite glass. Nat Pub Group. 2017;7:1–11.
13. Walas M, Piotrowski P, Lewandowski T, Synak A, Łapiński M, Sadowski W. Tailored white light emission in Eu^{3+}/Dy^{3+} doped tellurite glass phosphors containing Al^{3+} ions. Opt Mater. 2018;79:289–95.
14. Rada S, Culea E. FTIR spectroscopic and DFT theoretical study on structure of europium–phosphate–tellurate glasses and glass ceramics. J Mol Struct. 2009;929:141–8.
15. McLaughlin JC, Tagg SL, Zwanziger JW. The structure of alkali tellurite glasses. J Phys Chem B. 2001;105:67–75.
16. Devi ChBA, Mahamuda SK, Swapna K, Venkateswarlu M, Rao AS, Prakash GV. Pr^{3+} ions doped single alkali and mixed alkali fluoro tungsten tellurite glasses for visible red luminescent devices. J Non-Cryst Solids. 2018;498:345–51.
17. Rivera VAG, Ledemi Y, El-Amraoui M, Messaddeq Y, Marega E. Green-to-red light tuning by up-conversion emission via energy transfer in Er^{3+}–Tm^{3+}-codoped germanium–tellurite glasses. J Non-Cryst Solids. 2014;392–93:45–50.
18. Lin H, Liu K, Pun EYB, Ma TC, Peng X, An QD. Infrared and visible fluorescence in Er^{3+}-doped gallium tellurite glasses. Chem Phys Lett. 2004;398:146–50.
19. Tang Y, Liu Y, Cai P, Maalej R, Seo HJ. Thermal stability and spectroscopic properties of Ho^{3+} doped tellurite-borate glasses. J Rare Earths. 2015;33:939–45.
20. Tong TH, Yan X, Duan ZCh, Liao M, Suzuki T, Ohishi Y. Novel tellurite-phosphate composite microstructured optical fibers for nonlinear applications. Proc SPIE. 2012;9:2598–601.
21. Jha A, Richards BDO, Jose G, Fernandez TT, Hill CJ, Lousteau J. Review on structural, thermal, optical and spectroscopic properties of tellurium oxide based glasses for fibre optic and waveguide applications. Int Mater Rev. 2012;57:357–82.
22. Pach K, Golis E, Yousef ES, Sitarz M, Filipecki J. Structural studies of tellurite glasses doped with erbium ions. J Mol Struct. 2018;1164:32–3.

23. Kaur A, Khanna A, González-Barriuso M, González F, Chen B. Short-range structure and thermal properties of alumino-tellurite glasses. J Non-Cryst Solids. 2017;470:14–8.
24. Gupta N, Khanna A. Glass and anti-glass phase co-existence and structural transitions in bismuth tellurite and bismuth niobium tellurite systems. J Non-Cryst Solids. 2018;481:594–603.
25. Kaur A, Khanna A, Kaur A, Hirdesh, Gonzàlez-Barriuso M, Gonzàlez F. Effects of annealing on density, glass transition temperature and structure of tellurite, silicate and borate glasses. J Non-Cryst Solids. 2018;500:443–52.
26. Kacem IB, Gautron L, Coillot D, Neuville DR. Structure and properties of lead silicate glasses and melts. Chem Geol. 2017;461:104–14.
27. Munoz F, Munoz-Senovilla L. A model for the construction of the network in phosphate glasses through viscosity-structure relationships. J Non-Cryst Solids. 2017;471:142–5.
28. Wang R. Structure and luminescent property of Er^{3+}-doped germanate glasses. J Non-Cryst Solids. 2014;383:200–4.
29. Tagiara NS. Synthesis, thermal and structural properties of pure TeO_2 glass and zinc-tellurite glasses. J Non-Cryst Solids. 2017;457:116–25.
30. Kaur A, Khanna A, Aleksandrov LI. Structural, thermal, optical and photo-luminescent properties of barium tellurite glasses doped with rare-earth ions. J Non-Cryst Solids. 2017;476:67–74.
31. Luo Y, Zhang J, Sun J, Lu S, Wanh X. Spectroscopic properties of tungsten–tellurite glasses doped with Er^{3+} ions at different concentrations. Opt Mater. 2006;28:255–68.
32. Frechero MA, Quinzani OV, Pettigross RS, Villar M, Montani RA. IR absorption spectra of lithium and silver vanadium–tellurite based glasses. J Non-Cryst Solids. 2007;353:2919–25.
33. Pan Z, Morgan SH. Optical transitions of Er^{3+} in lead-tellurium-germanate glasses. J Lumin. 1997;75:301–8.
34. Gao S, Liu X, Kang S, Liao M, Hu L. 2-3 um emission and fluorescent decaying behavior in Ho^{3+}-doped tellurium germanate glass. Opt Mater. 2016;53:44–7.
35. Gao S, Kuan P, Li X, Wang L, Liao M, Hu L. Tm^{3+}-doped tellurium germanate glass and its double-cladding fiber for 2 μm laser. Mater Lett. 2015;143:60–2.
36. Jadach R, Zmojda J, Kochanowicz M, Miluski P, Lesniak M, Soltys M, Pisarska J. Spectroscopic properties of rare earth doped germanate glasses. Proc SPIE. 2018;10683:1068316.
37. Wang X. Direct observation of bulk second-harmonic generation inside a glass slide with tightly focused optical fields. Phys Rev B. 2016;93:161109-1–5.
38. Augustyn E, Żelechower M, Stróż D, Chrapoński J. The microstructure of erbium–ytterbium co-doped oxyfluoride glass–ceramic optical fibers. Opt Mater. 2012;34:944–50.
39. Kozhukharov V, Bürger H, Neov S, Sidzhimov B. Atomic arrangement of a zinc–tellurite glass. Polyhedron. 1986;5:771–7.
40. Jha A. Kinetics of glass-formation of heavy-metal fluoride melts. J Non-Cryst Solids. 1991;134:157–68.
41. Linganna K, Narro-García R, Desirena H, De la Rosa E, Basavapoornima Ch, Venkatramu V. Effect of P_2O_5 addition on structural and luminescence properties of Nd^{3+}-doped tellurite glasses. J Alloys Compd. 2016;684:322–7.
42. Konishi T, Hondo T, Araki T, Nishio K, Tsuchiya T, Matsumoto T. Investigation of glass formation and color properties in the P_2O_5–TeO_2–ZnO system. J Non-Cryst Solids. 2003;324:58–66.
43. Lu ZP, Liu CT. A new glass-forming ability criterion for bulk metallic glasses. Acta Mater. 2002;50:3501–12.
44. Lu ZP, Liu CT. Glass formation criterion for various glass-forming systems. Phys Rev. 2003;91:115505.
45. Kumar P, Bindra KS, Suri N, Thangaraj R. Transport properties of a-SnxSb20Se80-x ($8 \leq x \leq 18$) chalcogenide glass. J Phys D Appl Phys. 2006;39:642–6.
46. Chol-Lyong J, Lei X, Ding D, Yuan-Du D. Glass formation ability and kinetics of the $Gd_{55}Al_{20}Ni_{25}$ bulk metallic glass. Chin Phys Lett. 2006;23(3):672–4.
47. Aljihmani L, Vassilev V, Petkov P. Compositional trends of the physico-chemical properties in pseudoternary chalcogenide glasses. J Optoelectron Adv Mater. 2003;5:1187–92.
48. Avramov I, Zanotto ED, Prado MO. Glass-forming ability versus stability of silicate glasses. II. Theoretical demonstration. J Non-Cryst Solids. 2003;320:9–20.
49. Nasciemento ML, Souza FLA, Ferreira EB, Zanotto ED. Can glass stability parameters infer glass forming ability. J Non-Cryst Solids. 2005;351:3296–308.
50. Abdel-Kaber A, El-Mallawany R, ElKholy MM. Network structure of tellurite phosphate glasses: optical absorption and infrared spectra. J Appl Phys. 1993;73:71–4.
51. Brow R. Review: the structure of simple phosphate glasses. J Non-Cryst Solids. 2000;263–264:1–8.
52. Horea C, Toderas M, Ardelean I. Structural investigation of MnO-P_2O_5-TeO_2 glasses by FTIR spectroscopy. J Optoelectron Adv Mater. 2007;9:708–10.
53. Whittles Z, Marple M, Hung I, Gan Z, Sen S. Structure of BaO-TeO_2 glasses: a two-dimensional ^{125}Te NMR spectroscopic study. J Non-Cryst Solids. 2018;481:282–8.
54. Sidek A, Shaharuddin R, Talib ZA, Kamari HM, Daud WM. Synthesis and optical properties of ZnO-TeO_2 glass system. Am J Appl Sci. 2009;6:1489–94.
55. Sidek A, Shaharuddin R, Azmi BZ, Sharii Ah. Effect of ZnO on the thermal properties of tellurite glass. Adv Condens Matter Phys. 2013;2013:783207.
56. Sekiya T, Mochida N, Ohtsuka A. Raman spectra of MO-TeO_2 (M = Mg, Sr, Ba and Zn) glasses. J Non-Cryst Solids. 1994;168:106–14.
57. Sokolov V, Plotnichenko V, Koltashev V. Structure of barium chloride-oxide tellurite glasses. J Non-Cryst Solids. 2009;355:1574–84.